Nuclear Engineering and Technology 49 (2017) 1369–1378

Contents lists available at ScienceDirect

Nuclear Engineering and Technology

journal homepage: www.elsevier.com/locate/net

Original Article

Adaptive group of ink drop spread: a computer code to unfold neutron noise sources in reactor cores

Seyed Abolfazl Hosseini [a], Iman Esmaili Paeen Afrakoti [b, *]

[a] Department of Energy Engineering, Sharif University of Technology, Tehran, 8639-11365, Iran
[b] Faculty of Engineering & Technology, University of Mazandaran, P.O. Box 416, Pasdaran Street, Babolsar 47415, Iran

ARTICLE INFO

Article history:
Received 18 February 2017
Received in revised form
26 April 2017
Accepted 30 May 2017
Available online 17 July 2017

Keywords:
AGIDS
Neutron Noise
Noise source
Unfolding
Vibrating Absorber

ABSTRACT

The present paper reports the development of a computational code based on the Adaptive Group of Ink Drop Spread (AGIDS) for reconstruction of the neutron noise sources in reactor cores. AGIDS algorithm was developed as a fuzzy inference system based on the active learning method. The main idea of the active learning method is to break a multiple input–single output system into a single input–single output system. This leads to the ability to simulate a large system with high accuracy. In the present study, vibrating absorber-type neutron noise source in an International Atomic Energy Agency-two dimensional reactor core is considered in neutron noise calculation. The neutron noise distribution in the detectors was calculated using the Galerkin finite element method. Linear approximation of the shape function in each triangle element was used in the Galerkin finite element method. Both the real and imaginary parts of the calculated neutron distribution of the detectors were considered input data in the developed computational code based on AGIDS. The output of the computational code is the strength, frequency, and position (X and Y coordinates) of the neutron noise sources. The calculated fraction of variance unexplained error for output parameters including strength, frequency, and X and Y coordinates of the considered neutron noise sources were 0.002682 #/cm^{3}s, 0.002682 Hz, and 0.004254 cm and 0.006140 cm, respectively.

1. Introduction

In the safety analysis of reactor cores, it is very important to recognize the symptoms of an impending accident that may lead to an accident in the reactor core. One of the methods of identification of such symptoms is neutron noise analysis, in which fluctuations are identified through the neutron noise recorded in detectors. These fluctuations may be induced by small variations of the absorption, scattering, or fission cross sections of the materials in the reactor core. Neutron noise is the result of small variations of the neutron flux distribution due to the mentioned fluctuations. The obtained neutron noise distribution of the detectors in the reactor core may be utilized for reconstruction of neutron noise sources. Diagnosis of neutron noise sources such as control rod vibrations via neutron noise analysis methods was the subject of a number of prior studies and experiments. Various algorithms such as inversion, zoning, and scanning have been used for identification and localization of neutron noise sources such as unseated fuel assemblies in the reactor core, absorbers of variable strength, or vibration of core internals in pressurized water reactors [1–3]. The unfolding of a neutron noise source through the inverse method includes the solution of the inverse problem, in which the coefficient matrix is usually singular or badly scaled. The direct solution of the inverse problem leads to results with low accuracy (the accuracy of the localization of the neutron noise source is approximately 15 cm). Because just a limited number of the detectors are present in the reactor core, data on neutron noise are not available at all considered points (meshes) when using the inverse method. Therefore, to match the size of the measured neutron noise distribution and the calculated coefficient matrix in the inverse problem, interpolation is performed to obtain neutron noise values at all considered meshes. This interpolation leads to more error in the unfolding of the neutron noise source. The zoning method is another algorithm that may be used to unfold neutron noise source. In the zoning method, the reactor core is divided into certain zones, and the inverse method is used for determination of the neutron noise source in each zone. A comparison between the

* Corresponding author.
E-mail address: i.esmaili.p@umz.ac.ir (I.E.P. Afrakoti).

http://dx.doi.org/10.1016/j.net.2017.05.009

reconstructed neutron noise sources in each zone gives the actual neutron noise source. The error induced from the interpolation is slightly less than that when using the inverse method; however, the accuracy of the unfolded neutron noise source when using the zoning method is low. The scanning method is developed based on using a comparison of the neutron noise recorded in the detectors and the calculated responses (neutron noise) due to the possible locations of the neutron noise source in the reactor core. Scanning of all possible locations of the neutron noise source and minimizing of the difference between the detector readings and the calculated neutron noise due to possible sources gives the actual neutron noise source. Dividing the reactor core into certain zones (in the zoning method) and scanning of the reactor core (in the scanning method) lead to high running time (a few hours) for the reconstruction of the neutron noise source [1,2]. An artificial neural network (ANN) is another approach that may be used to unfold noise sources with acceptable accuracy (accuracy of the localization of the neutron noise source is between 5 cm and 10 cm) [4]. This is a mathematical algorithm inspired by biological neural networks. In the reported studies, using the developed algorithm based on ANNs, the neutron noise source was localized with accuracy close to 10 cm [5,6]. In the mentioned studies, the neutron noise sources of a type of absorber of variable strength or of a vibrating absorber were localized simply using the neural network, without the identification of other characteristics of the neutron noise source such as the strength and frequency. In a paper previously published by the first author of the present paper [4], computational codes developed based on the ANN were used for reconstruction of noise sources (all characteristics of neutron noise source) for types of absorber of variable strength and for a vibrating absorber with good accuracy (accuracy of 0.1–10 cm in the localization of the neutron noise source). A literature review of the studies performed on noise source unfolding shows that a neural network or a combination of a neural network and the scanning method are more accurate in comparison to the other aforementioned algorithm [4].

In the present study, a new algorithm based on the Adaptive Group of Ink Drop Spread (AGIDS) is proposed to unfold, with high accuracy, the noise source of a type of vibrating absorber in the IAEA (International Atomic Energy Agency)- two dimensional (2D) reactor core (accuracy between 0.001 cm and 9 cm in the localization of the neutron noise source). The input data (neutron noise distribution in the detectors) of the developed computer code have been calculated using the previously developed DYN-FEMG computational code [7].

An outline of the remainder of the present paper is as follows. In Section 2, we briefly introduce the mathematical formulation used for the calculation of the neutron noise distribution in the reactor core. The main specifications of the IAEA-2D reactor core are presented in Section 3. In Section 4, the developed computational code based on AGIDS and the unfolded neutron noise source using the mentioned computer code are presented. The results of the neutron noise calculation and a reconstruction of the neutron noise source is presented in Section 5. A discussion of the results and the merits of the proposed method is presented in Section 6. Finally, Section 7 gives the concluding remarks.

2. Methodology for simulation of neutron noise distribution

In the present study, a first-order approximation of the neutron noise diffusion equation in two energy groups is considered to calculate the neutron noise distribution due to the neutron noise source. The general form of the mentioned equation, obtained by considering the neutron noise source as fluctuations in the scattering, absorption, and fission macroscopic cross sections, is presented as Eq. (1) [1–4,8]:

$$\left[\nabla.\overline{\overline{D}}(\bar{r})\nabla+\overline{\overline{\Sigma}}_{\mathrm{dyn}}(\bar{r},\omega)\right]\times\begin{bmatrix}\delta\varphi_1(\bar{r},\omega)\\ \delta\varphi_2(\bar{r},\omega)\end{bmatrix}= \overline{\varphi}_{s,1\to2}(\bar{r})\,\delta\Sigma_{s,1\to2}(\bar{r},\omega)+\overline{\overline{\varphi}}_a(\bar{r})\begin{bmatrix}\delta\Sigma_{a,1}(\bar{r},\omega)\\ \delta\Sigma_{a,2}(\bar{r},\omega)\end{bmatrix}+ \overline{\overline{\varphi}}_f(\bar{r},\omega)\begin{bmatrix}\delta\nu_1\Sigma_{f,1}(\bar{r},\omega)\\ \delta\nu_2\Sigma_{f,2}(\bar{r},\omega)\end{bmatrix}, \tag{1}$$

where all quantities are defined as usual and the matrices and vectors are expressed as Eqs. (2–5):

$$\overline{\overline{\Sigma}}_{\mathrm{dyn}}(\bar{r},\omega)=\begin{bmatrix}-\Sigma_1(\bar{r},\omega) & \dfrac{\nu_2\Sigma_{f,2}(\bar{r})}{k_{\mathrm{eff}}}\left(1-\dfrac{i\omega\beta_{\mathrm{eff}}}{i\omega+\lambda}\right)\\ \Sigma_{s,1\to2}(\bar{r}) & -\left(\Sigma_{a,2}(\bar{r})+\dfrac{i\omega}{\nu_2}\right)\end{bmatrix} \tag{2}$$

$$\overline{\varphi}_{s,1\to2}(\bar{r})=\begin{bmatrix}\varphi_1(\bar{r})\\ -\varphi_1(\bar{r})\end{bmatrix} \tag{3}$$

$$\overline{\overline{\varphi}}_a(\bar{r})=\begin{bmatrix}\varphi_1(\bar{r}) & 0\\ 0 & \varphi_2(\bar{r})\end{bmatrix} \tag{4}$$

$$\overline{\overline{\varphi}}_f(\bar{r},\omega)=\begin{bmatrix}-\varphi_1(\bar{r})\left(1-\dfrac{i\omega\beta_{\mathrm{eff}}}{i\omega+\lambda}\right) & -\varphi_2(\bar{r})\left(1-\dfrac{i\omega\beta_{\mathrm{eff}}}{i\omega+\lambda}\right)\\ 0 & 0\end{bmatrix} \tag{5}$$

The coefficient $\Sigma_1(\bar{r},\omega)$ used in Eq. (2) is defined as Eq. (6):

$$\Sigma_1(\bar{r},\omega)=\Sigma_{r,1}(\bar{r})+\frac{i\omega}{\nu_1}-\frac{\nu_1\Sigma_{f,1}(\bar{r})}{k_{\mathrm{eff}}}\left(1-\frac{i\omega\beta_{\mathrm{eff}}}{i\omega+\lambda}\right) \tag{6}$$

To calculate the neutron noise source term on the right-hand side of Eq. (1) (Eqs. 3–5), the neutron flux distribution should be calculated from the solution of the neutron diffusion equation. To this end, the neutron flux distribution obtained from the previously developed computational code is used to calculate the neutron noise source term [7]. In the present study, a vibrating absorber type neutron noise source is assumed. The Green function technique is used [2] to calculate the neutron noise distribution, in which the neutron noise distribution due to the unit value of the point noise source in the reactor core is calculated. The point source may be located in any considered triangle element. Therefore, the Green components due to different positions of the unit value-point noise sources are calculated via the solution of Eq. (7):

$$\left[\nabla.\overline{\overline{D}}(\bar{r})\nabla+\overline{\overline{\Sigma}}_{\mathrm{dyn}}(\bar{r},\omega)\right]\times\begin{bmatrix}G_{g\to1}\left(\bar{r},\bar{r}',\omega\right)\\ G_{g\to2}\left(\bar{r},\bar{r}',\omega\right)\end{bmatrix}= \begin{bmatrix}\delta\left(\bar{r}-\bar{r}'\right)\\ 0\end{bmatrix}_{g=1}\quad or\quad \begin{bmatrix}0\\ \delta\left(\bar{r}-\bar{r}'\right)\end{bmatrix}_{g=2} \tag{7}$$

where $G_{g\to1}(\bar{r},\bar{r}',\omega)$ and $G_{g\to2}(\bar{r},\bar{r}',\omega)$ are the Green function components of energy groups 1 and 2 at position $\bar{r}$, induced by the noise source in group g located at position $\bar{r}'$. It is possible to consider the neutron noise source in the fast or thermal energy group.

If the noise source is considered to be in the thermal energy group (a perturbation in the thermal macroscopic cross section), Eq. (7) can be written as Eqs. (8) and (9) using the Galerkin finite element method (GFEM):

$$\sum_{e=1}^{E}\Bigg[\iint_{\Omega^{(e)}} D_1\,\nabla N^{(e)}(\bar{r})\nabla N^{(e)T}(\bar{r})G_{2\to1}^{(e)}- \Sigma_1^{(e)}\iint_{\Omega^{(e)}} \mathrm{d}\Omega N^{(e)}(\bar{r})N^{(e)T}(\bar{r})G_{2\to1}^{(e)}+ \frac{\nu_2\Sigma_{f,2}^{(e)}}{k_{\mathrm{eff}}}\left(1-\frac{i\omega\beta_{\mathrm{eff}}}{i\omega+\lambda}\right)\iint_{\Omega^{(e)}}\mathrm{d}\Omega\, N^{(e)}(\bar{r})N^{(e)T}(\bar{r})G_{2\to2}^{(e)}+ \int_{\partial\Omega^{(e)V}}\mathrm{d}sN^{(e)}(\bar{r})N^{(e)T}(\bar{r})\frac{G_{2\to1}^{(e)}}{2}\Bigg]=0, \tag{8}$$

$$\sum_{e=1}^{E}\Bigg[\iint_{\Omega^{(e)}}\mathrm{d}\Omega\, D_2\nabla N^{(e)}(\bar{r})\nabla N^{(e)T}(\bar{r})G_{2\to2}^{(e)}+ \Sigma_{s,1\to2}^{(e)}\iint_{\Omega^{(e)}}\mathrm{d}\Omega\, N^{(e)}(\bar{r})N^{(e)T}(\bar{r})G_{2\to1}^{(e)}- \left(\Sigma_{a,2}^{(e)}+\frac{i\omega}{v_2}\right)\iint_{\Omega^{(e)}}\mathrm{d}\Omega\, N^{(e)}(\bar{r})N^{(e)T}(\bar{r})G_{2\to1}^{(e)}+ \int_{\partial\Omega^{(e)V}}\mathrm{d}s\, N^{(e)}(\bar{r})N^{(e)T}(\bar{r})\frac{G_{2\to2}^{(e)}}{2}\Bigg]=\begin{bmatrix}N_i^{(e)}(\bar{r})\\ N_j^{(e)}(\bar{r})\\ N_k^{(e)}(\bar{r})\end{bmatrix}, \tag{9}$$

where $N_i^{(e)}$, $N_j^{(e)}$ and $N_k^{(e)}$ are the components of the shape function in GFEM.

In Eq. (8), the differential parts were transformed by applying the Divergence's theorem, as in Eq. (10):

$$\int_{\Omega^{(e)}}\mathrm{d}\Omega\, N^{(e)}(\bar{r})\ \left(-D_1\,\nabla^2N^{(e)T}(\bar{r})G_{2\to1}^{(e)}\right)= \int_{\Omega^{(e)}}\mathrm{d}A\,\nabla N^{(e)}(\bar{r}).\nabla N^{(e)T}(\bar{r})G_{2\to1}^{(e)}- \int_{\Omega^{(e)}}\mathrm{d}\Omega\,\nabla.(N^{(e)}(\bar{r})\,\nabla N^{(e)T}(\bar{r})G_{2\to1}^{(e)}= \int_{\Omega^{(e)}}\mathrm{d}\Omega\,\nabla N^{(e)}(\bar{r}).\,\nabla N^{(e)T}(\bar{r})G_{2\to1}^{(e)}- \int_{\partial\Omega^{(e)V}+\partial\Omega^{(e)R}}\mathrm{d}s\,N^{(e)}(\bar{r})\,\frac{\partial N^{(e)T}(\bar{r})G_{2\to1}^{(e)}}{\partial n} \tag{10}$$

where $\partial\Omega^{(e)\mathrm{V}}$and $\partial\Omega^{(e)\mathrm{R}}$ refer to the boundary length with vacuum and the perfect reflective boundary conditions (BCs) for element e, respectively.

Also,

$$\frac{\partial N^{(e)T}(\bar{r})G_{2\to1}^{(e)}}{\partial n}=\nabla N^{(e)T}(\bar{r})G_{2\to1}^{(e)}.\,\bar{n} \tag{11}$$

where $\bar{n}$ is the normal unit vector of the volume V. Two types of BCs are considered. The first BC is the one with no incoming neutrons at vacuum boundaries (Marshak BC), which is expressed as Eq. (12):

$$\frac{\partial N^{(e)T}(\bar{r})G_{2\to1}^{(e)}}{\partial n}=-\frac{N^{(e)T}(\bar{r})G_{2\to1}^{(e)}}{2D_g} \tag{12}$$

The second BC is zero net current or a perfect reflective BC, which is described by Eq. (13):

$$\frac{\partial N^{(e)T}(\bar{r})G_{2\to1}^{(e)}}{\partial n}=0 \tag{13}$$

The same procedure for applying the BC is considered in Eq. (9). No incoming current and perfect reflection are the common BCs that are used in the solution of the neutron diffusion equation.

The Green function components in each energy group in different triangle elements are calculated from the solution of Eqs. (8) and (9). Finally, the fast and thermal neutron noise distributions are calculated via integration over the multiplying of the Green function components by the noise source in the whole domain of the reactor core, as in Eq. (14):

$$\begin{bmatrix}\delta\varphi_1(\bar{r},\omega)\\ \delta\varphi_2(\bar{r},\omega)\end{bmatrix}=\begin{bmatrix}\int\left[G_{1\to1}\left(\bar{r},\bar{r}',\omega\right)S_1\left(\bar{r}',\omega\right)+\right.\\ \int\left[G_{2\to1}\left(\bar{r},\bar{r}',\omega\right)S_2\left(\bar{r}',\omega\right)\right]\mathrm{d}\bar{r}'\\ \int\left[G_{1\to2}\left(\bar{r},\bar{r}',\omega\right)S_1\left(\bar{r}',\omega\right)+\right.\\ \int\left[G_{2\to2}\left(\bar{r},\bar{r}',\omega\right)S_2\left(\bar{r}',\omega\right)\right]d\bar{r}'\end{bmatrix} \tag{14}$$

If only the thermal macroscopic absorption cross section is perturbed, Eq. (14) will be reduced as Eq. (15):

$$\begin{bmatrix}\delta\varphi_1(\bar{r},\omega)\\ \delta\varphi_2(\bar{r},\omega)\end{bmatrix}=\begin{bmatrix}\int\left[G_{2\to1}\left(\bar{r},\bar{r}',\omega\right)S_2\left(\bar{r}',\omega\right)\right]\mathrm{d}\bar{r}'\\ \int\left[G_{2\to2}\left(\bar{r},\bar{r}',\omega\right)S_2\left(\bar{r}',\omega\right)\right]\mathrm{d}\bar{r}'\end{bmatrix} \tag{15}$$

Here, it is assumed that the noise source is only located in the thermal energy group and the neutron noise distribution in the reactor core is calculated using the aforementioned equations.

Because adjoint noise distribution may be used as the response of the detectors in the reactor core, it is essential in any noise analysis of the reactor core to calculate the adjoint noise. To this end, one can obtain the matrix equation of the adjoint neutron noise by assuming a point source located at position r_0. The matrix form of the adjoint noise equations can be expressed as in Eq. (16) [7]:

$$\left[\nabla.\overline{\overline{D}}(\bar{r})\nabla+\overline{\overline{\Sigma}}_{\mathrm{dyn}}^{\dagger}(\bar{r},\omega)\right]\times\begin{bmatrix}\delta\varphi_1^{\dagger}(\bar{r},\omega)\\ \delta\varphi_2^{\dagger}(\bar{r},\omega)\end{bmatrix}=\begin{bmatrix}\delta(\bar{r}-\bar{r}_0)\\ \delta(\bar{r}-\bar{r}_0)\end{bmatrix} \tag{16}$$

where $\delta\varphi_1^{\dagger}(\bar{r},\omega)$ and $\delta\varphi_2^{\dagger}(\bar{r},\omega)$ are the fast and thermal adjoint noises, respectively. $\overline{\overline{\Sigma}}_{\mathrm{dyn}}^{\dagger}(\bar{r},\omega)$ is the transpose of the dynamical matrix $\overline{\overline{\Sigma}}_{\mathrm{dyn}}(\bar{r},\omega)$. In addition, $\delta(\bar{r}-\bar{r}_0)$ refers to the Dirac delta function at position $\bar{r}_0$.

Like the direct neutron noise calculations, the Green function technique and GFEM are applied for the solution of the adjoint noise calculations. Fast and thermal adjoint noises are the results of these calculations.

For the modeling of the vibrating absorber-type noise source, the obtained adjoint Green function components for the noise source of the type of absorber of variable strength are used [1,7]. In this case, the induced neutron noise at position r_0 can be determined using Eq. (17):

$$\begin{bmatrix}\delta\varphi_1(\bar{r}_0,\omega)\\ \delta\varphi_2(\bar{r}_0,\omega)\end{bmatrix}=\gamma.\bar{\varepsilon}(\omega).\nabla_{\mathrm{rs}}\left[G_{\delta\Sigma_{\mathrm{a}}}^{\dagger}(\bar{r}_{\mathrm{s}},\bar{r}_0\,,\omega)\right] \tag{17}$$

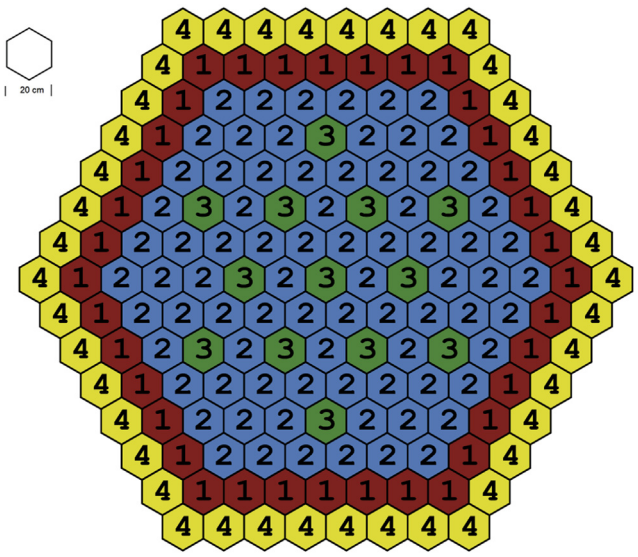

Fig. 1. Core configuration of the IAEA-2D reactor core. IAEA, International Atomic Energy Agency.

Table 1
Material cross section of each assembly in IAEA-2D reactor core.

	M1	M2	M3	M4
D_1 (cm)	1.500	1.500	1.500	1.500
D_2 (cm)	0.400	0.400	0.400	0.400
$\nu\Sigma_{f,1}$ (cm^{-1})	0.000	0.000	0.000	0.000
$\nu\Sigma_{f,2}$ (cm^{-1})	0.135	0.135	0.135	0.000
$\Sigma_{R,1}$ (cm^{-1})	0.030	0.030	0.030	0.040
$\Sigma_{R,2}$ (cm^{-1})	0.080	0.085	0.130	0.010

D1 and D2 are neutron diffusion coefficients in 1 and 2 energy groups, respectively. Mi denotes to assembly type. $\nu\Sigma f,1,;\ \nu\Sigma f,2$ are the macroscopic fission cross section in the 1 and 2 energy groups, respectively. Also, $\Sigma R,1$ and $\Sigma R,2$ are neutron removal cross in the 1 and 2 energy groups, respectively.

where the vector $\bar{\varepsilon}(\omega)$ describes the 2D vibrations of the noise source at frequency ω around its equilibrium position, which is located at r_s. Here, the operator ∇_{rs} is the derivative of the adjoint Green function with respect to the first variable. As can be seen in Eq. (17), if one wants to estimate the response of a single detector, it is more advantageous to use the adjoint approach instead of the forward one. By contrast, if determination of the neutron noise in several positions is needed, only the forward approach is applicable [1,7]. In such a case, the derivative of the forward Green function with respect to the second variable is required and the neutron noise induced by the vibrating absorber type of noise source can be calculated as:

$$\begin{bmatrix}\delta\varphi_1(\bar{r},\omega)\\ \delta\varphi_2(\bar{r},\omega)\end{bmatrix} = \gamma.\bar{\varepsilon}(\omega).\nabla_{rs}\left[G_{\delta\Sigma_a}(\bar{r},\bar{r}_s,\omega)\right] \tag{18}$$

Compared to Eq. (17), calculating the derivative of the forward Green function with respect to the second variable is more complicated, because the full space dependence of the adjoint Green function with respect to the first variable is known, whereas this is not the case for the forward one.

3. Main specification of the benchmark problem

In the present study, the calculation is performed for IAEA-2D benchmark problems in two energy group approximations. Fig. 1 displays the core configuration of the IAEA-2D reactor core. The BCs of the reactor core include no incoming current for the external boundaries. Table 1 represents the material cross section of each assembly in the IAEA-2D reactor core. The IAEA-2D reactor is an IAEA benchmark proposed by the Argonne Code Center.

4. Unfolding of neutron noise source using AGIDS as a fuzzy modeling algorithm

In all fields of engineering, in order to understand and analyze the behavior of a system, a proper modeling technique is usually developed. The constructed model can be used for better understanding of the underlying mechanisms of the system, the design of new processes, or the design of controllers. In most systems, the mathematical relationship among system inputs, state variables, and system outputs cannot be obtained, or it is difficult to develop such a model. Exact information about the input–output relationships and system characteristics is not usually readily available. Fuzzy modeling can be applied in such situations to extract a proper model based on the available vague data. The linguistic fuzzy model developed by Mamdani extracts available qualitative knowledge of

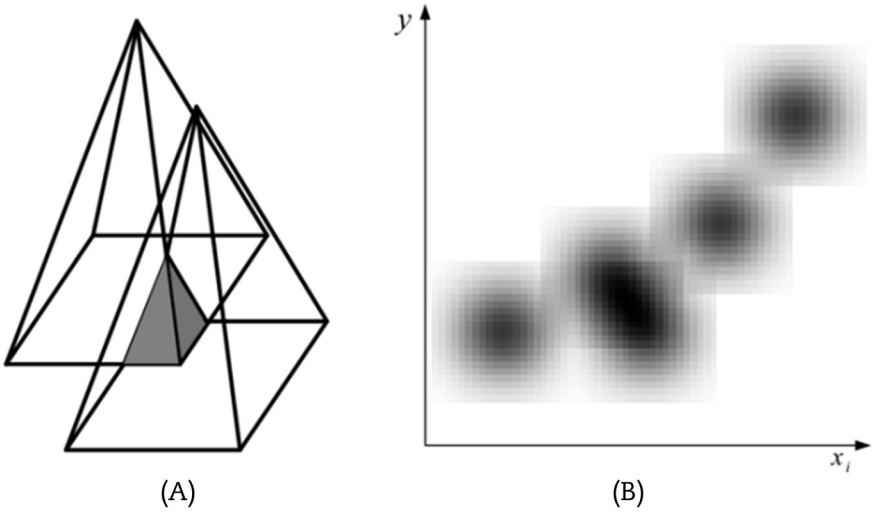

Fig. 2. Sample data diffused on IDS plane. (A) Two pyramid-shaped ink stains with overlap. (B) Applying IDS operator for five sets of sample data on IDS plane. IDS, ink drop spread.

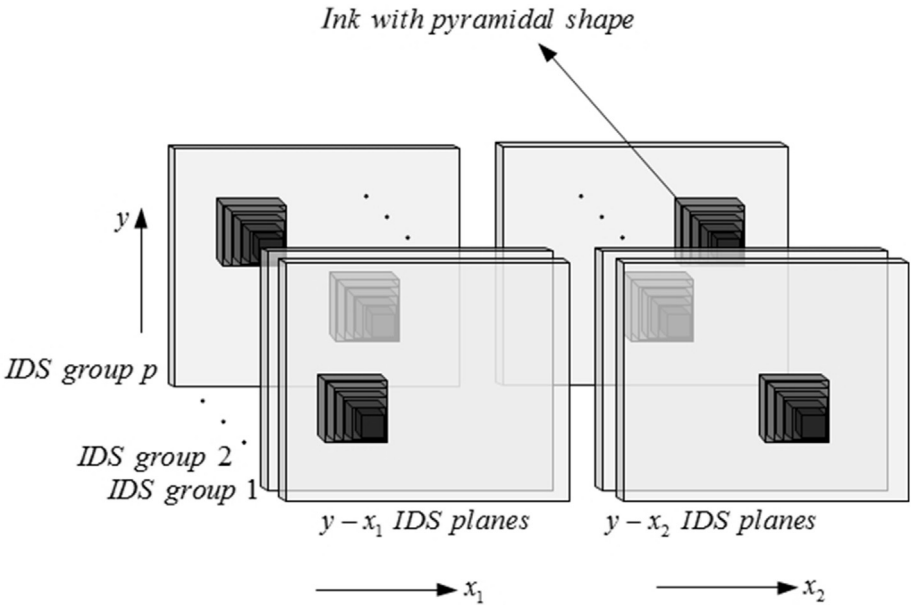

Fig. 3. IDS groups for a two inputs and one output system with p sample data simulation procedure. IDS, ink drop spread.

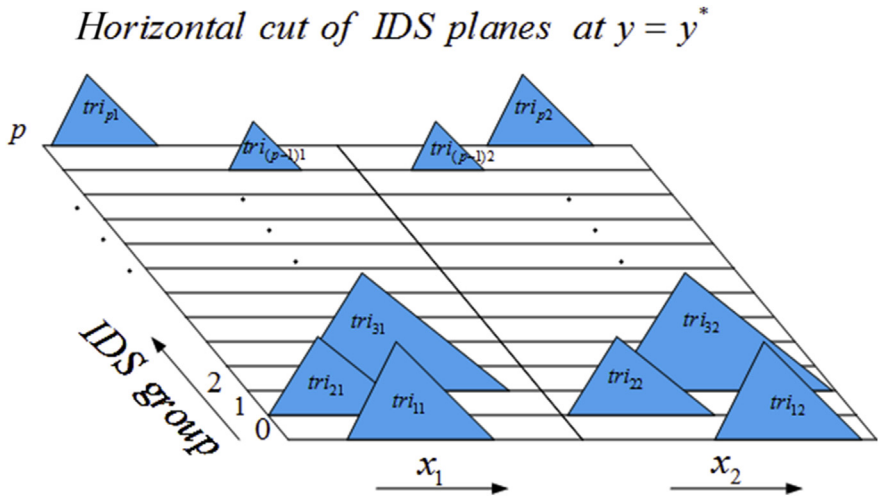

Fig. 4. Result of horizontal cut of the IDS plane. IDS, ink drop spread.

the system in terms of if–then rules [9,10]. An instant Mamdani rule is presented in Eq. (19):

$$R_i\text{: If } \bar{x} \text{ is } A_i, \text{ then } y \text{ is } B_i; \quad i = 1, 2, \ldots, k; \tag{19}$$

In the antecedent part, $\bar{x}$ is the input linguistic variable, A_i is the vector of the antecedent linguistic fuzzy sets or concepts, y is the output linguistic variable, and B_i is the vector of the consequent linguistic term. Expert knowledge should be extracted in order to form such linguistic rules. Depending on the problem, proper inference and defuzzification algorithms should be used to find the output based on the input and these rules. The Takagi–Sugeno (TS) model [11] uses a crisp function of the input variables in the consequent part; this is in contrast to the Mamdani model, which uses linguistic if–then rules with fuzzy propositions in both the antecedent and consequent parts. The TS model, therefore, is a combination of mathematical and linguistic regression-based modeling, in which the antecedent describes the fuzzy regions in the input space in which the consequent function is valid. It should be noted that in the TS model, a proper optimization algorithm is needed to tune the parameters of the consequent function.

The AGIDS algorithm was developed in 2016 by Afrakoti et al. [12] based on the active learning method (ALM) algorithm as a fuzzy inference system [12]. The main idea of the ALM algorithm is to break a multiple input–single output (MISO) system into a certain single input–single output (SISO) system [13]. Each SISO system is modeled by an ink drop spread (IDS) plane. Construction of an IDS plane is done by mapping the training data on the output versus input plane by application of the IDS operator. Application of the IDS operator will diffuse the training data on the IDS plane. The IDS operator places a pyramid-shaped stain on each set of training data, (x, y), on the IDS plane. Aggregation is done for points at which the ink drops overlap with each other. In Fig. 2, five sets of sample data are diffused on an IDS plane using a pyramid-shaped IDS operator.

Although ALM shows high performance in many applications such as systems modeling, pattern classification, and control [14–16], it has several drawbacks such as complex hardware

implementation and the need for an effective optimization algorithm. Numerous studies have been done to solve these drawbacks [17–19].

AGIDS is a sample-based algorithm that models the system with local information. For each set of training data, an IDS group will be formed. For a system with n inputs, each IDS group consists of n IDS planes that were formed using the IDS operator. In Fig. 3, the IDS groups are shown for the two input–one output systems with p training data.

Until this step, it is the structure of the model that is constructed. For calculation of the output for a test input, the inference rule of the model can be extracted by applying a horizontal cut to the IDS groups in a quantized output level such as y^*. In Fig. 4, the result of such a horizontal cut is shown. Each triangle is part of a pyramid-shaped ink stain dropped on the relevant page. Using this plane, the inference rule of the AGIDS structure for a sample cut at y^* will be as follows:

If x_1 is tri_{y^*11} AND x_2 is tri_{y^*12} OR
If x_1 is tri_{y^*21} AND x_2 is tri_{y^*22} OR …
If x_1 is tri_{y^*p1} AND x_2 is tri_{y^*p2}, then $y = y^*$

If the n quantized level is considered for the output variable, there will be n rules, as in the equation above. Computing the output for a set of input test data can be done by applying a T-norm operator to the confidence degree of all planes in an IDS group to each quantized level of the output variables; then, an S-norm operator should be applied to the result of the antecedent parts off all IDS groups. So, the output of the model will be a vector that

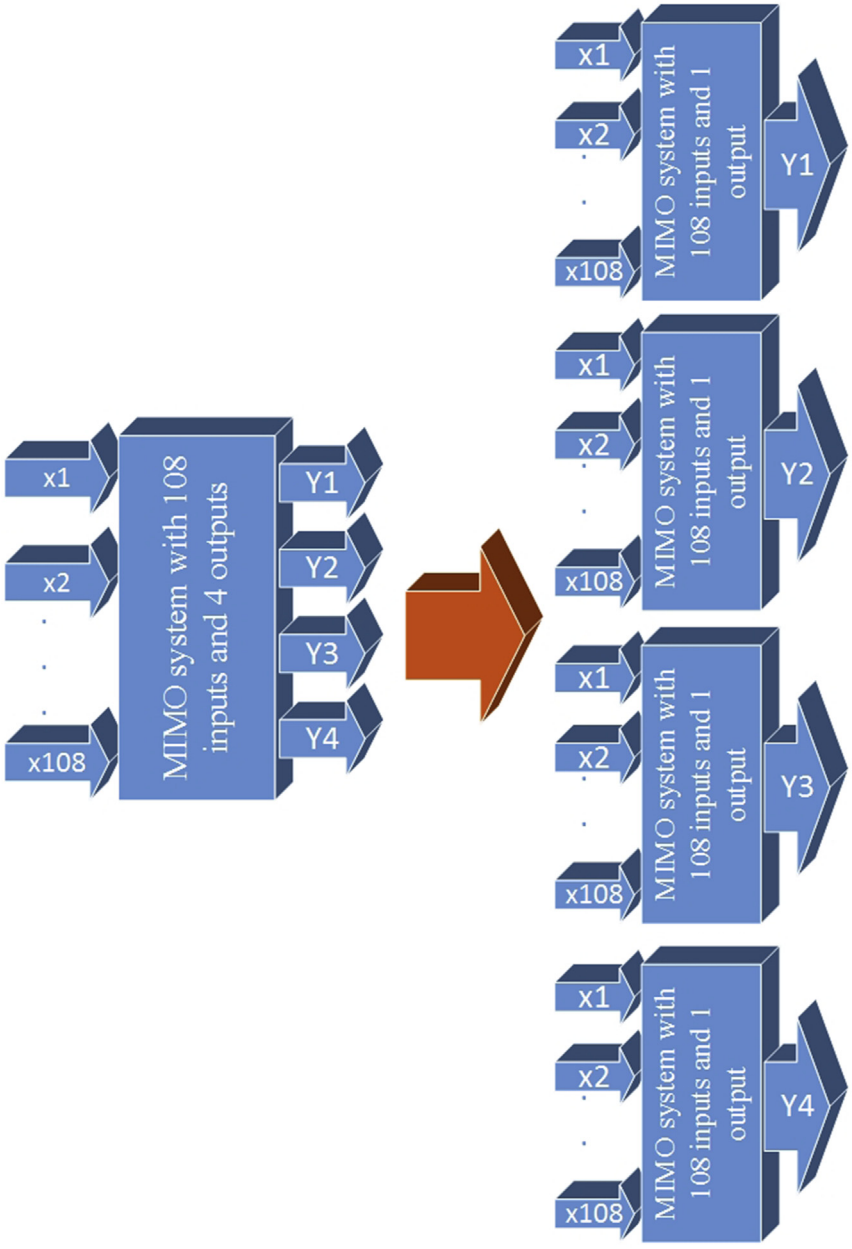

Fig. 5. MIMO system with 108 inputs and four outputs is broken into four MISO systems with 108 inputs and one output. MIMO, multiple input–multiple output system; MISO, multiple input–single output system, X; Y.

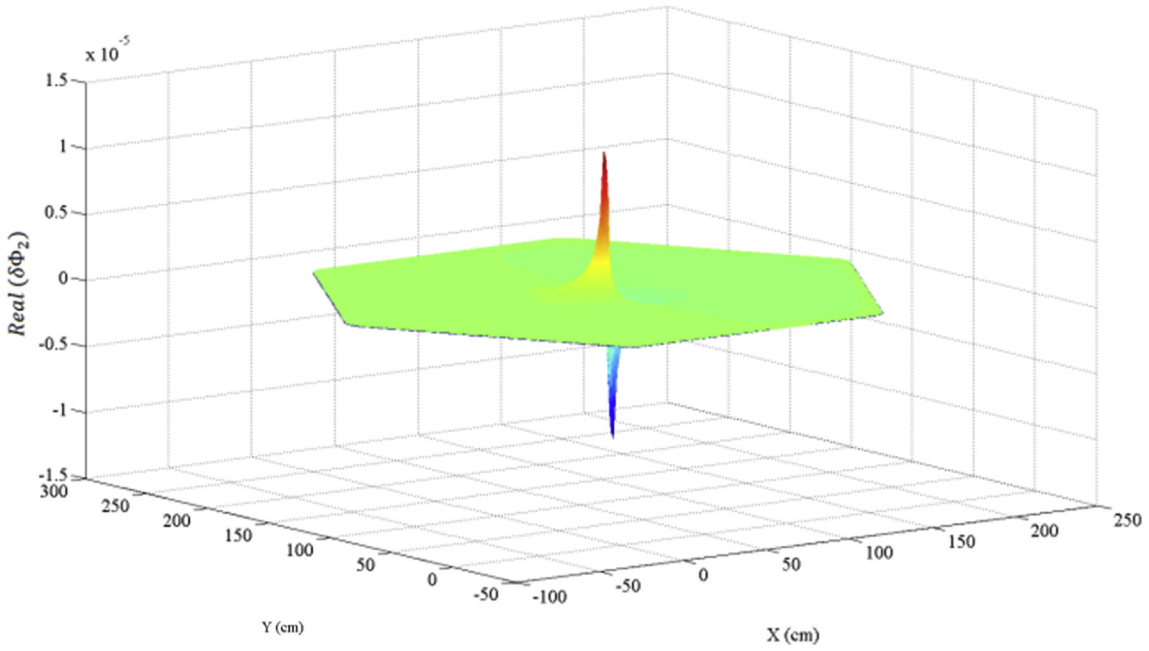

Fig. 6. Real part of the thermal neutron noise due to vibrating absorber-type neutron noise source.

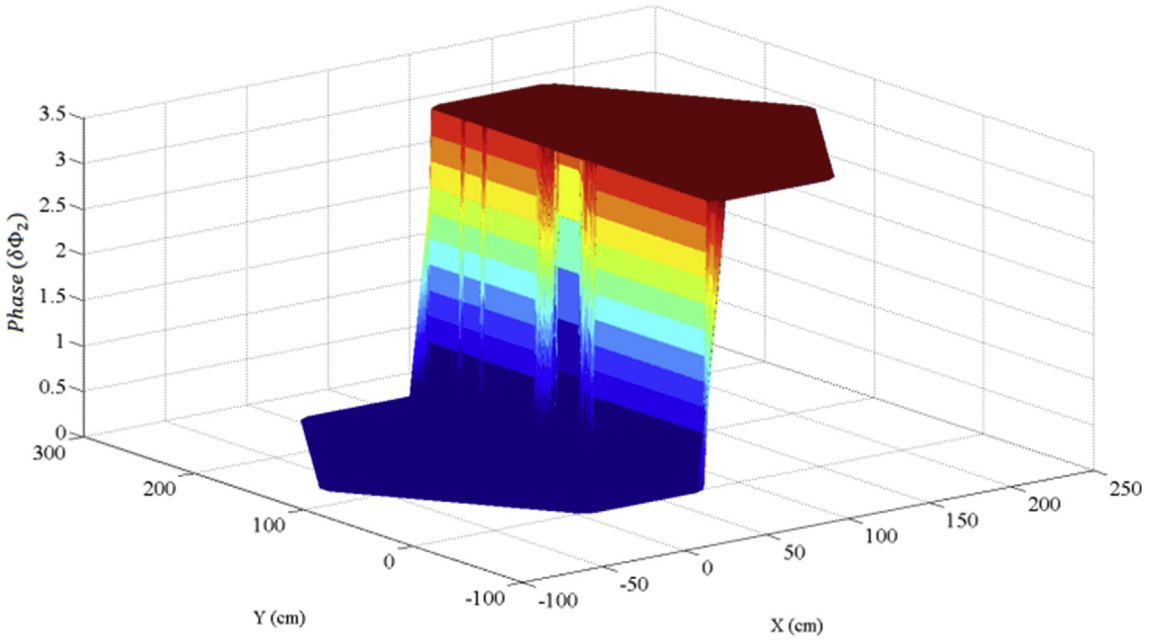

Fig. 7. Phase of the thermal neutron noise due vibrating absorber type neutron noise source.

contains the confidence degree of the constructed model for each quantized level of the output variables, which are fuzzy numbers. Transforming the output fuzzy number to a crisp value can be done by using a suitable defuzzification algorithm such as the weighted average formula.

AGIDS has very few parameters, but these parameters include the radius of the ink stains and the resolution of the IDS planes. No complex optimization is needed to tune these parameters and a simple try and error algorithm can be used for this purpose. AGIDS has proved itself in complex classification and modeling problems with respect to powerful ANN algorithms such as multilayer perceptron (MLP) and adaptive-network-based fuzzy inference system (ANFIS).

Because the AGIDS algorithm is designed to model an MISO system, applying it in this problem requires that four AGIDS models be constructed, as shown in Fig. 5. Each model is used to develop a relation between the input variables and one of the output variables. Each model is designed as a system with 108 inputs and one output variable. The resolution of the quantization is set to 256 levels and the ink stain radius is set to 15. Gaussian shape ink stains

Table 2
Comparison between unfolded and actual values of X coordinate (cm) for 51 randomly considered noise sources.

Actual	Unfolded	Actual	Unfolded	Actual	Unfolded
162.205	161.267	−27.444	−27.533	86.863	90.467
158.442	157.333	−63.499	−74.733	90.741	98.333
55.077	55.067	151.061	149.467	32.090	27.533
149.619	149.467	−7.862	−7.867	49.260	51.133
110.415	110.133	133.733	133.733	125.583	125.867
90.473	90.467	37.831	31.467	43.268	43.267
105.894	102.267	125.760	125.867	−42.403	−43.267
110.133	110.133	−27.444	−27.533	66.867	66.867
133.733	133.733	17.879	15.733	−18.540	−19.667
−30.277	−31.467	102.290	102.267	−27.444	−27.533
−63.499	−74.733	86.175	86.533	−30.286	−31.467
201.307	208.467	4.274	3.933	133.783	133.733
180.407	180.933	83.916	90.467	45.284	39.333
137.667	137.667	61.825	66.867	47.835	27.533
149.465	157.333	168.487	169.133	205.099	216.333
70.394	74.733	3.933	3.933	19.585	19.667
−19.645	−19.667	95.552	98.333	−19.065	−19.667

Table 3
Comparison between the unfolded and actual values of Y coordinate (cm) for 51 randomly considered noise sources.

Actual	Unfolded	Actual	Unfolded	Actual	Unfolded
158.016	157.333	87.135	90.467	86.533	86.533
−38.807	−39.333	3.933	3.933	149.476	149.467
19.667	19.667	193.727	192.733	3.933	3.933
107.212	102.267	7.060	7.867	161.012	161.267
39.502	39.333	161.245	161.267	−19.645	−19.667
172.897	173.067	162.235	161.267	19.946	19.667
−19.253	−19.667	110.409	110.133	88.911	98.333
25.715	19.667	55.241	66.867	27.224	43.267
45.103	43.267	19.584	19.667	121.958	121.933
57.435	74.733	184.003	184.867	184.003	184.867
54.855	55.067	95.553	98.333	−49.541	−51.133
137.352	137.667	19.949	19.667	41.327	39.333
−52.127	−55.067	145.510	145.533	180.407	180.933
7.866	7.867	145.508	145.533	139.949	145.533
−19.645	−19.667	−3.933	−3.933	171.835	173.067
145.533	145.533	54.865	55.067	157.324	157.333
−19.645	−19.667	98.333	98.333	86.533	86.533

are used in this problem. A total of 5,000 samples are used for training and testing of the algorithm. Seventy percent of the data are chosen for construction of the models and to form the IDS groups in the training phase; 30% of the data are used for testing the algorithm in the modeling task. The regression coefficient and the fraction of variance unexplained (FVU) index are used for evaluation of the proposed algorithm.

Table 4
Comparison between unfolded and actual values of the noise source strength (#/cm^3 s) for 51 randomly considered noise sources.

Actual	Unfolded	Actual	Unfolded	Actual	Unfolded
0.013625	0.013636	0.001522	0.001285	0.005716	0.005693
0.015149	0.015688	0.002630	0.002618	0.010114	0.010086
0.013507	0.013525	0.014876	0.015131	0.010302	0.010308
0.009673	0.009648	0.010302	0.010301	0.011375	0.011385
0.014216	0.014260	0.001305	0.000724	0.001059	0.000284
0.014834	0.015067	0.001219	0.000477	0.006706	0.006698
0.004693	0.004704	0.001633	0.001397	0.001638	0.001406
0.003967	0.003679	0.005656	0.005902	0.012755	0.012757
0.001856	0.001741	0.010425	0.010409	0.013985	0.014004
0.004143	0.004038	0.001400	0.001129	0.009614	0.009608
0.015149	0.015665	0.002746	0.002747	0.007030	0.007010
0.003383	0.003426	0.009229	0.009237	0.002631	0.002630
0.011497	0.011482	0.002215	0.002156	0.008094	0.008105
0.001271	0.000659	0.001361	0.000970	0.014570	0.014709
0.012688	0.012725	0.015287	0.015965	0.014263	0.014315
0.015118	0.015589	0.009873	0.009873	0.004189	0.004185
0.015149	0.015689	0.003472	0.003526	0.008225	0.008230

Table 5
Comparison between unfolded and actual values of the noise source frequency (Hz) for 51 randomly considered noise sources.

Actual	Unfolded	Actual	Unfolded	Actual	Unfolded
0.084687	0.084758	0.008327	0.006832	0.034789	0.034642
0.094303	0.097706	0.015320	0.015245	0.062534	0.062359
0.083941	0.084058	0.092577	0.094187	0.063724	0.063762
0.059754	0.059594	0.063724	0.063715	0.070491	0.070553
0.088414	0.088693	0.006955	0.003295	0.005406	0.000517
0.092315	0.093788	0.006414	0.001731	0.041036	0.040985
0.028332	0.028406	0.009030	0.007540	0.009061	0.007596
0.023750	0.021936	0.034408	0.035964	0.079197	0.079214
0.010437	0.009710	0.064501	0.064396	0.086961	0.087079
0.024864	0.024202	0.007555	0.005845	0.059379	0.059345
0.094302	0.097559	0.016051	0.016055	0.043075	0.042952
0.020069	0.020339	0.056949	0.057003	0.015324	0.015321
0.071260	0.071165	0.012702	0.012330	0.049791	0.049858
0.006745	0.002884	0.007311	0.004843	0.090649	0.091529
0.078775	0.079010	0.095174	0.099448	0.088711	0.089039
0.094104	0.097076	0.061018	0.061014	0.025151	0.025131
0.094303	0.097707	0.020629	0.020968	0.050621	0.050648

The FVU index is defined in Eq. (20). In this formula, $\vec{x}_i$ is the input vector of the ith set of sample data, y is the real output value, $\hat{y}$ is the output of constructed model, N is the number of data points and $\bar{y}$ is average of output variables.

FVU is a kind of normalized error index. In an FVU index, the ratio of the absolute value of error with respect to the amount of an output variable's variation is important. The best modeling result will be for FVU = 0.

$$\mathrm{FVU} = \frac{\sum_{i=1}^{N}\left(\hat{y}(\vec{x}_i) - y(\vec{x}_i)\right)^2}{\sum_{i=1}^{N}\left(y(\vec{x}_i) - \bar{y}(\vec{x}_i)\right)^2} \tag{20}$$

5. Results

To prepare the data for the noise source unfolding section, the neutron noise distributions in the reactor core due to the 5,000 randomly generated noise sources are calculated (each set of data includes the randomly generated frequency, strength, and X and Y coordinates of the noise source). The neutron noise distributions in the reactor core due to each considered noise source are calculated using the developed DYN-FEMG computer code [7]. As a sample, the magnitude and phase of the calculated neutron noise distribution due to the variable strength noise source of the absorber located in the central area of the reactor core are displayed in Figs. 6 and 7, respectively. The validation of the neutron noise distribution calculated through three different approaches using the developed computational code was presented in previously published papers [7,20,21]. The validated neutron noise distribution is used as input data for the noise source reconstruction.

The real and imaginary parts of the neutron noise calculated in the 54 detectors in the reactor core (108 inputs for each data) are considered inputs of the developed computational code based on the AGIDS algorithm. The position (X and Y coordinates), strength, and frequency of the noise source are the outputs of the developed computational code. Table 2 shows comparisons between the unfolded X coordinate of the neutron noise source and the actual coordinate for the 51 randomly considered samples. Similar comparisons for the Y coordinate, the strength, and the frequency at which the noise source of the vibrating absorber occurred are given in Tables 3–5, respectively. Table 6 shows the regression coefficients of the predicted output versus actual output for the four outputs of the system computed from the 1,500 considered testing

Table 6
Regression coefficient and average error of the predicted output determined using the developed computer code based on AGIDS algorithm versus actual values.

Characteristic of the noise source	Strength	Frequency	*X*	*Y*
Regression coefficient	0.9994	0.9994	0.9985	0.9988
FVU	0.002682	0.002682	0.004254	0.006140

AGIDS, Adaptive Group of Ink Drop Spread; FVU, fraction of variance unexplained.

samples by the AGIDS algorithm. The regression coefficient is a touchstone for the evaluation of any regression problem. This criterion is used to evaluate the performance of the AGIDS algorithm. Also, Table 6 displays the FVU errors of the output parameters obtained from the 1,500 considered testing samples. As can be seen, there is excellent agreement between the unfolded noise source and the actual noise source.

6. Discussion

In the present study, a vibrating absorber-type neutron noise source was unfolded using a computer code developed based on the AGIDS algorithm. The DYN-FEMG computer code [7] was used to calculate the neutron noise distribution of considered noise source. The 5,000 randomly generated noise sources including the 5,000 randomly generated locations (*X* and *Y* coordinates), strength, and frequency of the noise source, and the corresponding calculated neutron noise values (real and imaginary parts) in the 54 detectors in the reactor core are the outputs and inputs of the computer code developed based on AGIDS. In previously published papers, the unfolding of an absorber of a variable strength noise source was performed using inversion, zoning, and scanning algorithms [2,20]. The scanning algorithm unfolds the noise source with good accuracy in the absence of background noise in the reactor core. Therefore, the scanning algorithm is much more reliable than the inversion (and to a lesser extent, zoning) algorithms [20]. This can be explained by the fact that no matrix inversion is needed for unfolding, whereas the inversion (and to a lesser extent zoning) algorithms rely on the inversion of a matrix, which might be badly scaled under certain circumstances. The drawback of the scanning algorithm is that it requires long running time to develop the computer code [2,20]. Also, the scanning method gives no information about the frequency at which the noise source occurs. The best accuracy of localization of neutron noise sources using algorithms such as the inverse and zoning algorithms is close to 15 cm [2,20]. The frequency of the neutron noise source cannot be reconstructed using the inverse and zoning methods. In the algorithm developed based on ANNs, by Tambouratzis and Antonopoulos-Domis [6], the neutron noise source was localized with accuracy close to 10 cm. In a previously published work by the first author, results for a noise source unfolded using the ANN were presented [4]. In the mentioned study, the frequency, strength, and position of the noise source were reconstructed with good accuracy (accuracy of 0.1–10 cm in the localization of the neutron noise source) using a method based on the logsig and tansig transfer functions. The motivation of the present study was the development of a computer code that could reconstruct the neutron noise source with high accuracy (accuracy of 0.001–9 cm in localization of the neutron noise source). As shown in Tables 2 and 3, the accuracy of the location of the unfolded noise source in the present study is better than those in similar published works (accuracy on the order of 0.001 with running time on the order of 30 s) [5,6]. In fact, a vibrating absorber-type neutron noise source was localized with high accuracy in the present study, whereas the average error of the localization of the noise source in similar published works is almost 10 cm [6]. All characteristics of the noise source, including the strength, occurrence frequency, and position of the noise source in the reactor core, were estimated with high accuracy.

7. Conclusion

In the present study, a vibrating absorber-type neutron noise source in the IAEA-2D reactor core was reconstructed using the developed computational code, which is based on the AGIDS algorithm. The calculation of the neutron noise distribution in the reactor core was performed using the developed DYN-FEMG computer code. Four characteristics of the noise source, including the strength, frequency, and location of the noise source, were identified with high accuracy. The computational code, developed based on the AGIDS algorithm, may be considered a reliable tool for identification of neutron noise sources in reactor cores. Therefore, it may be introduced as an important computer code in the noise and safety analysis of reactor cores.

Conflicts of interest

There is no conflict of interests.

Acknowledgments

The first author is grateful to the Iran National Science Foundation, which has supported the present research (95820334).

References

[1] I. Pázsit, O. Glöckler, On the neutron noise diagnostics of PWR control rod vibration: I. Periodic vibrations, Nucl. Sci. Eng. 85 (1984) 167–177.
[2] C. Demazière, G. Andhill, Identification and localization of absorbers of variable strength in nuclear reactors, Ann. Nucl. Energy 32 (2005) 812–842.
[3] M.M.R. Williams, Random Processes in Nuclear Reactors, Pergamon Press Ltd, Headington Hill Hall, Oxford, 2013.
[4] S.A. Hosseini, N. Vosoughi, Noise source reconstruction using ANN and hybrid methods in VVER-1000 reactor core, Prog. Nucl. Energy 71 (2014) 232–247.
[5] N.S. Garis, I. Pázsit, U. Sandberg, Determination of PWR control rod position by core physics and neural network methods, Nucl. Technol. 123 (1998) 278–295.
[6] T. Tambouratzis, M. Antonopoulos-Domis, Instability localization with artificial neural networks (ANNs), Ann. Nucl. Energy 29 (2002) 235–253.
[7] S.A. Hosseini, N. Vosoughi, Neutron noise simulation by GFEM and unstructured triangle elements, Nucl. Eng. Des. 253 (2012) 238–258.
[8] S. Itoh, A fundamental study of neutron spectra unfolding based on the maximum likelihood method, Nucl, Instrum. Methods Phys. Res. Sect. A 251 (1986) 144–155.
[9] L. Zedeh, Outline of a new approach to the analysis of complex systems and decision processes, IEEE Trans. Syst. Man Cybern. 3 (1973) 28–44.
[10] E.H. Mamdani, Application of fuzzy logic to approximate reasoning using linguistic synthesis, in: Proceedings of the Sixth International Symposium on Multiple-valued Logic, IEEE Computer Society Press, 1976.
[11] T. Takagi, M. Sugeno, Fuzzy identification of systems and its applications to modeling and control, IEEE Trans. Syst. Man Cybern. SCM-15 (1985) 116–132.
[12] I.E.P. Afrakoti, S.B. Shouraki, F.M. Bayat, M. Gholami, Using a memristor crossbar structure to implement a novel adaptive real-time fuzzy modeling algorithm, Fuzzy Sets Syst. 307 (2016) 115–128.
[13] S.B. Shouraki, N. Honda, Recursive fuzzy modeling based on fuzzy interpolation, J. Adv. Comput. Intell. 3 (1999) 114–125.
[14] M. Murakami, N. Honda, A study on the modeling ability of the IDS method: a soft computing technique using pattern-based information processing, Int. J. Approx. Reason 45 (2007) 470–487.
[15] M. Firouzi, S.B. Shouraki, I.E.P. Afrakoti, Pattern analysis by active learning

method classifier, J. Intell. Fuzzy Syst. 26 (2014) 49–62.
[16] Y. Sakurai, A Study of the Learning Control Method Using PBALM—a Nonlinear Modeling Method, PhD, University of Electro-Communications, Tokyo, 2005.
[17] I.E.P. Afrakoti, S.B. Shouraki, B. Haghighat, An optimal hardware implementation for active learning method based on memristor crossbar structures, IEEE Syst. J. 8 (2014) 1190–1199.
[18] I.E.P. Afrakoti, A. Ghaffari, S.B. Shouraki, Effective partitioning of input domains for ALM algorithm in pattern recognition and image analysis (PRIA), in: 2013 First Iranian Conference on, IEEE, 2013.
[19] H. Sagha, S.B. Shouraki, H. Beigy, H. Khasteh, E. Enayati, Genetic ink drop spread, in: Intelligent Information Technology Application, IITA'08, Second International Symposium on, IEEE, 2008.
[20] S.A. Hosseini, N. Vosoughi, On a various noise source reconstruction algorithms in VVER-1000 reactor core, Nucl. Eng. Des. 261 (2013) 132–143.
[21] S.A. Hosseini, N. Vosoughi, Development of 3D neutron noise simulator based on GFEM with unstructured tetrahedron elements, Ann. Nucl. Energy 97 (2016) 132–141.